THE ASTROPHYSICAL JOURNAL, 563:806–815, 2001 December 20

PULSAR WIND NEBULAE IN EVOLVED SUPERNOVA REMNANTS

JOHN M. BLONDIN
Department of Physics, North Carolina State University, Raleigh, NC 27695
ROGER A. CHEVALIER
Department of Astronomy, University of Virginia, P.O. Box 3818, Charlottesville, VA 22903
AND
DARGAN M. FRIERSON
Department of Mathematics, Princeton University, Princeton, NJ 08544
Received 2001 July 4; accepted 2001 August 27

ABSTRACT

For pulsars similar to the one in the Crab Nebula, most of the energy input to the surrounding wind nebula occurs on a timescale $\lesssim 10^3$ yr; during this time, the nebula expands into freely expanding supernova ejecta. On a timescale $\sim 10^4$ yr, the interaction of the supernova with the surrounding medium drives a reverse shock front toward the center of the remnant, where it crushes the pulsar wind nebula (PWN). We have carried out one- and two-dimensional, two-fluid simulations of the crushing and reexpansion phases of a PWN. We show that (1) these phases are subject to Rayleigh-Taylor instabilities that result in the mixing of thermal and nonthermal fluids, and (2) asymmetries in the surrounding interstellar medium give rise to asymmetries in the position of the PWN relative to the pulsar and explosion site. These effects are expected to be observable in the radio emission from evolved PWN because of the long lifetimes of radio-emitting electrons. The scenario can explain the chaotic and asymmetric appearance of the Vela X PWN relative to the Vela pulsar without recourse to a directed flow from the vicinity of the pulsar. The displacement of the radio nebulae in G327.1−1.1, MSH 15−56 (G326.3−1.8), G0.9+0.1, and W44 relative to the X-ray nebulae may be due to this mechanism. On timescales much greater than the nebular crushing time, the initial PWN may be mixed with thermal gas and become unobservable, so that even the radio emission is dominated by recently injected particles.

Subject headings: pulsars: general — shock waves — supernova remnants
On-line material: color figures

1. INTRODUCTION

Pulsars are expected to be born inside massive stars, so that the evolution of the wind nebulae that they produce is expected to depend on a number of different factors: the structure of the supernova, the nature of the surrounding medium, the evolution of the pulsar spin-down power, and the space velocity of the pulsar. The evolution of pulsar nebulae can be divided into a number of phases that are important for their observational appearance (Reynolds & Chevalier 1984, hereafter RC84; Chevalier 1998). Initially, the pulsar nebula expands into the freely expanding supernova ejecta. The pulsar provides a constant wind power, and the swept-up shell of ejecta is accelerated. Jun (1998) has carried out two-dimensional simulations of the Rayleigh-Taylor instabilities that occur during this phase, with the aim of modeling the Crab Nebula. On a timescale of $\sim 10^3$ yr for a pulsar like the Crab, the power input from the pulsar drops steeply so that the nebula expands adiabatically. The expansion approaches free expansion within the supernova.

The next phase of evolution results from the interaction of the supernova remnant with the surrounding medium and the inward motion of the reverse shock front that is driven by this interaction. On a timescale of $\sim 10^4$ yr, the reverse shock makes its way back to the center of the remnant. The pulsar nebula that has been created by the early energy injection is compressed during this phase. Because of the synchrotron losses of high-energy particles, this nebula is best observed at radio wavelengths. At the same time, the continued wind power from the pulsar can create a nebula, including high-energy emission, that is localized to the pulsar. If the pulsar has a velocity of 100s of kilometers per second, as is quite likely for a normal pulsar (Lyne & Lorimer 1994), a bow shock nebula can form around the pulsar and this nebula can separate from the crushed nebula from the earlier phase.

RC84 made some approximate estimates of the effects of crushing a pulsar nebula by the external supernova remnant, with an emphasis on the synchrotron luminosity. Van der Swaluw et al. (2001) carried out one-fluid, one-dimensional simulations of the crushing process, finding that there are considerable transient effects before the nebula settles into a slow expansion. Our aim here is also to investigate the hydrodynamics of the interaction, with attention to instabilities. In § 2 we present the basic parameters that are needed to model the pulsar nebula/supernova remnant interaction. A difference with the work of van der Swaluw et al. (2001) is that they assumed supernova ejecta with a constant density profile, whereas we allow for an outer power-law profile. Numerical simulations in one and two dimensions are presented in §§ 3 and 4, respectively. We allow for different adiabatic indices in the relativistic fluid and the thermal gas fluid. In the two-dimensional simulations, the effect of a density gradient in the external medium is treated in addition to a constant density ambient medium. We believe this situation is relevant to the Vela X

radio pulsar nebula in the Vela supernova remnant, which is discussed in § 5 along with other remnants. The conclusions are in § 6.

2. A MODEL FOR THE PWN/SNR INTERACTION

To investigate the dynamical evolution of the pulsar wind nebula/supernova remnant system beyond the free expansion phase, we have constructed a simple model based on the expanding pulsar bubble solution (Chevalier 1977) and the self-similar driven wave (Chevalier 1982). We begin by assuming the stellar material ejected by the Type II supernova is expanding ballistically ($r = vt$) and can be described by a steep outer power-law density profile inside of which the density is constant. The density profile is parameterized by the total mass of ejecta, $M_{\rm ej}$, the kinetic energy released in the supernova, $E_{\rm sn}$, and the density power-law exponent, n:

$$\rho_{\rm ej}(r, t) = \begin{cases} A v_t^n r^{-n} t^{n-3} & \text{for } r > v_t t\,, \\ A t^{-3} & \text{for } r < v_t t\,, \end{cases} \tag{1}$$

where the constant A is given by

$$A = \frac{5n - 25}{2\pi n} E_{\rm sn} v_t^{-5} \tag{2}$$

and the velocity at the intersection of the density plateau and the power law is given by

$$v_t = \left(\frac{10n - 50}{3n - 9} \frac{E_{\rm sn}}{M_{\rm ej}}\right)^{1/2}. \tag{3}$$

If we further assume that this ejecta is expanding into a uniform ambient medium with density ρ_a, the expansion of the supernova remnant is described by a self-similar solution given by Chevalier (1982). The radius of the forward shock, R_1, in this self-similar driven wave (SSDW) is given by (assuming $s = 0$ in Chevalier's notation)

$$R_1 = \alpha \left(\frac{A v_t^n}{\rho_a}\right)^{1/n} t^{(n-3)/n}\,, \tag{4}$$

where the constant $\alpha = 1.048$ for $n = 9$, but varies relatively little with the value of n. The assumption of a constant density surrounding medium may not generally apply because core collapse supernovae have massive star progenitors which are known to affect their surroundings through winds and photoionization. The timescale for the reverse shock wave to return to the center ($\sim 10^4$ yr) makes it plausible that the outer shock wave has proceeded to the interstellar medium. If a wind bubble has been created by the progenitor star, the inward motion of the reverse shock is modified.

The last component of the model, the pulsar wind nebula, is treated as an adiabatic wind bubble driven by a pulsar wind with a kinetic luminosity, L_p. If we use the standard approximation of an isobaric bubble bounded by a thin shell of swept up ambient gas, as in Chevalier (1977), the expansion of this bubble within the uniform (but decreasing with time) density of the ejecta is given by

$$R_p = 1.50 \left(\frac{n}{n-5}\right)^{1/5} \left(\frac{n-5}{n-3}\right)^{1/2} \left(\frac{E_{\rm sn}^3 L_p^2}{M_{ej}^5}\right)^{1/10} t^{6/5}\,. \tag{5}$$

This combined model is illustrated in Figure 1, which shows the radial profile of the density throughout the structure. The supernova ejecta is separated into three parts: a thin shell at R_p that has been swept up by the expanding pulsar bubble, cold freely expanding ejecta between R_p and the reverse SNR shock at R_2, and a thin shell of shocked ejecta at R_2 that has been decelerated by the reverse shock.

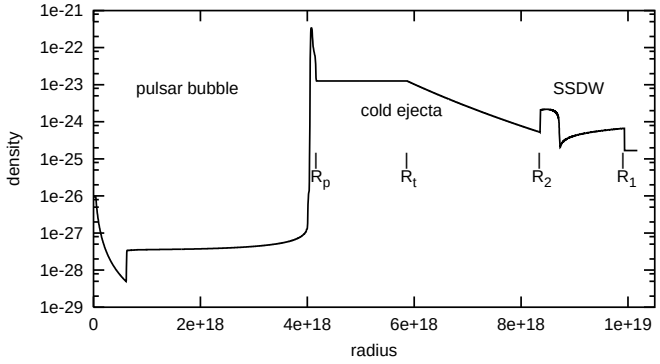

FIG. 1.—Density profile of our model for the interaction of a pulsar nebula with the host supernova remnant. The supernova remnant is modeled as a self-similar driven wave (SSDW) bounded by a forward shock at R_1 and a reverse shock at R_2. The pulsar bubble has swept up a thin shell of ejecta at R_p. The edge of the ejecta plateau at R_t is just about to reach R_2, after which the reverse shock will begin propagating in toward the center.

The discontinuity between R_2 and R_1 separates the shocked ejecta (*left*) and the shocked CSM (*right*). The discontinuity near $r = 0$ is the termination shock of the pulsar wind.

Several things will happen at an age of $\sim 10^3$ yr to change this model. First, the pulsar will die out. Without continued power input, the expansion of the pulsar nebula will slow down until it becomes frozen into the expanding ejecta. Second, the pulsar nebula will reach the edge of the plateau in the SN ejecta and begin accelerating down the steep density gradient. Alternatively, the plateau will reach the reverse shock of the SSDW. As the ram pressure at the reverse shock rapidly decays away, the reverse shock is driven toward the center of the remnant, resulting in a dynamical interaction with the pulsar nebula.

The exact ordering of these events depends on the parameters of the model described above, namely, $E_{\rm sn}$, $M_{\rm ej}$, n, ρ_a, L_p, and the lifetime of the pulsar. The time of the first event, the decline of the pulsar power, is determined by our model for $L_p(t)$. We approximate the power input from the pulsar by assuming a constant pulsar magnetic field and braking index p, which yields

$$L_p = L_{\rm pi} \left(1 + \frac{t}{\tau}\right)^{-(p+1)/(p-1)}, \tag{6}$$

where $L_{\rm pi}$ is the initial pulsar power and $p = 3$ for the magnetic dipole case. It can be seen that much of the power input occurs up to time τ, so that τ corresponds roughly to the lifetime of the pulsar. The initial pulsar power is given in terms of the initial spin period, P_i: $L_{\rm pi} = I\Omega_i^2/[(p-1)\tau]$, where I is the pulsar moment of inertia and $\Omega_i = 2\pi/P_i$ is the initial spin rate. For the Crab pulsar, p is measured to be 2.5 and $L_p = 4 \times 10^{38}$ ergs s^{-1}, which lead to $\tau = 744$ yr and $L_{\rm pi} = 3 \times 10^{39}$ ergs s^{-1} for $I = 10^{45}$ g cm^2 (e.g., Chevalier 1977 and references therein). The power input for our models C and D (see Table 1) is considerably above $L_{\rm pi}$ for the Crab pulsar, but corresponds to $P_i \approx 5$ ms (for $p = 3$), which is a plausible initial rotation period.

TABLE 1

MODEL PARAMETERS

PARAMETER	DEFINITION	UNITS	MODEL A	MODEL B	MODEL C	MODEL D	MODEL E
$L_{\rm pi}$	Pulsar luminosity	10^{40} ergs s^{-1}	1.0	0.1	5.0	5.0	1.0
τ.....	Pulsar lifetime	yr	500	500	500	500	2500
$M_{\rm ej}$	Mass of SN ejecta	$M_\odot$	8	4	16	8	8
$E_{\rm sn}$	Kinetic energy of SN	10^{51} ergs	1	1	1	1	1
n	Ejecta power law		9	9	9	9	9
ρ_a	Ambient density	m_p cm^{-3}	0.1	0.1	0.1	0.1	0.1

The second event, the pulsar nebula reaching the edge of the ejecta plateau, $R_t = v_t t$, occurs at

$$t_2 = 2.64\left(\frac{n-5}{n}\right)\frac{E_{\rm sn}}{L_p}, \tag{7}$$

assuming constant pulsar luminosity. If, however, the pulsar has already died away, the nebula will expand slower, and this will be an underestimate to t_2. The third event, the inward motion of the reverse shock, begins when the edge of the ejecta plateau reaches the reverse shock, i.e., $R_t = R_2$:

$$t_3 = B\left(\frac{A}{\rho_a}\right)^{1/3} \approx 120\left(\frac{M_{\rm ej}}{M_\odot}\right)^{5/6}\left(\frac{\rho_a}{m_p}\right)^{-1/3}\left(\frac{E_{\rm sn}}{10^{51}{\rm erg}}\right)^{-1/2} {\rm yr}, \tag{8}$$

where the numerical value is quoted for $n = 9$, for which $B = 0.688$.

Choosing reasonable parameters as listed in Table 1 for model A, we find $t_2 \approx 3700$ yr and $t_3 \approx 1500$ yr. Thus we expect the reverse shock to begin moving into the interior of the remnant, where it will encounter the pulsar nebula. For other parameters, however, this sequence may be reversed. For example, lowering $E_{\rm sn}$ by 3 would lead to $t_2 < t_3$; the lower energy means a slower expansion, requiring a longer time to sweep up mass but a shorter time for the pulsar to blow through the slower ejecta.

3. ONE-DIMENSIONAL HYDRODYNAMIC SIMULATIONS

To investigate the dynamical evolution of the pulsar nebula beyond the phase of self-similar expansion in a uniform ejecta, we employ numerical simulations that begin shortly before the PWN/SNR interaction. These simulations are computed with the VH-1 code, a Lagrangian-remap version of the piecewise parabolic method. The standard VH-1 code was adapted to treat two fluids with two different values of γ such that the pulsar wind can be modeled with $\gamma = 4/3$, while the supernova ejecta and circumstellar gas are modeled with $\gamma = 5/3$. The one-dimensional PWN/SNR model is evolved on a grid of 1000 radial zones that expands to follow the forward shock. Several simulations on a grids of 750 and 1500 zones produced almost identical results.

The initial conditions for the SSDW are taken from the solution described in Chevalier (1982), scaled to the parameters listed in Table 1 for model A. The initial conditions for the pulsar nebula are taken from a separate hydrodynamic simulation of a wind blown bubble in which the wind is an adiabatic gas with $\gamma = 4/3$, a mass loss rate $\dot{M}_w = 2L_p/v_p^2$, and a wind velocity, v_p, scaled to yield a sound speed in the shocked gas of $c/\sqrt{3}$, appropriate for a relativistic gas. The pulsar luminosity decays away according to equation (6) assuming a braking index of $p = 3$.

A more realistic model for the pulsar wind nebula would allow for a relativistic, MHD (magnetohydrodynamic) flow, as in the steady state model for the Crab Nebula by Kennel & Coroniti (1984a, 1984b). However, once the relativistic wind passes through the wind termination shock, the flow velocity drops to $c/3$. The bulk velocity is not relativistic in the nebula, although the shocked particles are highly relativistic. This situation can be approximated by a $\gamma = 4/3$ fluid. The magnetic field may be a more significant omission because the magnetic field in the Crab Nebula is thought to be in approximate equipartition with the particles. In particular, the magnetic field could affect the growth of instabilities at the edge of the pulsar nebula (Jun, Norman, & Stone 1995; Hester et al. 1996). The tangential magnetic field may be especially strong at the edge of the nebula (Emmering & Chevalier 1987). The magnetic field may inhibit the growth of the instability along the direction of the field, but has less of an effect across the field.

The evolution of the PWN/SNR model is illustrated with a space-time diagram in Figure 2. The evolution begins at $t \approx 2\tau$, just prior to the end of the SSDW phase at t_3. One can identify two bands of high-density gas in the early evolution: the pulsar nebula shell made up of swept up ejecta, and a shell of shocked ejecta on the trailing side of the SSDW. The simulation begins with the edge of the ejecta plateau reaching the reverse shock. The reverse shock and the shell of shocked ejecta then begin to push inward, but the SSDW does not have much time to react to the dropping ejecta density before the pulsar shell strikes it.

At an age of about $\sim$3000 yr the pulsar nebula shell collides with the dense SSDW shell. From this point on all of the ejecta is contained in a relatively thin shell (width $\sim 0.1\, R_1$) bounded by low-density shocked pulsar wind on the inside and by shocked circumstellar gas on the outside. This initial impact generates a strong shock wave transmitted through the SSDW. When this shock catches up with the forward shock there is an abrupt, but brief, acceleration of the forward shock, followed by a faster deceleration than in the SSDW phase. A weak reflected shock is also generated, which bounces back and forth through the pulsar bubble at the relatively high sound speed of $c/\sqrt{3}$. This bouncing wave can be seen as nearly vertical lines in the pressure image of Figure 2.

Following the collision of the pulsar and reverse SNR shocks, the thin shell of ejecta is gradually pushed inward with respect to the outer shock wave by the high pressure of the shocked CSM. Initially the pressure in the pulsar bubble is negligible, and the presence of the PWN has no effect on

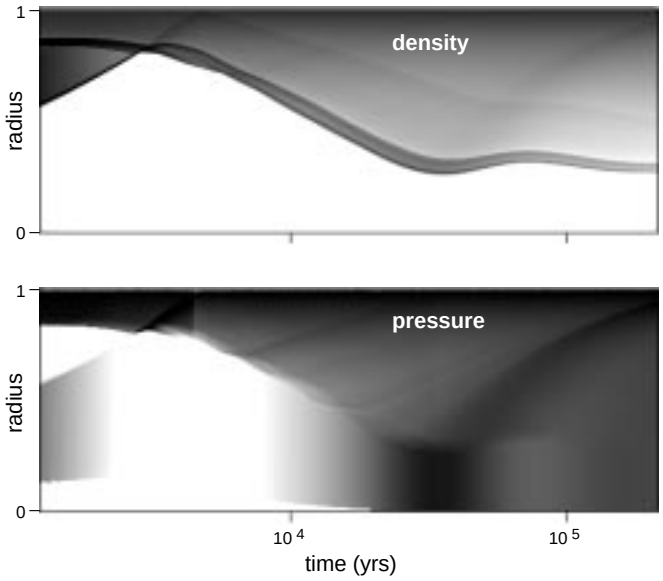

FIG. 2.—Evolution of the pulsar nebula within the host supernova remnant as computed with the one-dimensional hydrodynamics code for the parameters listed for model A. Both the density (*top*) and the pressure (*bottom*) are depicted in logarithmic scales, with black corresponding to high values and white to low values. The radial extent of the grid is scaled to follow the forward shock front, such that the location of the forward shock is a horizontal line near the top of each plot. [*See the electronic edition of the Journal for a color version of this figure.*]

the dynamics of the infalling reverse shock. But as the pulsar bubble is compressed, the interior pressure rises. For our nominal PWN/SNR parameters, the pressure in the bubble becomes comparable to the pressure behind the reverse shock once the PWN has been crushed to approximately half the radius of the SNR. Eventually the PWN reaches a minimum radius of 0.25 R_1 at an age of $\sim$35,000 yr. At this point the pressure of the compressed pulsar bubble accelerates the shell of shocked ejecta back out to a radius of 0.3 R_1. From this point on all of the ejecta remains in a thin shell with a width of $\sim$10% of R_1, slowly oscillating about an average radius of $\sim$0.27 R_1. The simulations of van der Swaluw et al. (2001) also show oscillations after the crushing phase.

The extent to which the pulsar bubble is compressed depends on the pressure in the bubble compared to the pressure behind the reverse shock as it propagates in toward the pulsar nebula. Assuming a constant pulsar luminosity and using the pressure behind the reverse shock in the SSDW phase, we find a ratio of pressures at a time of t_3:

$$\frac{P_b}{P_2} = 0.166 L_p^{2/5} M_{\rm ej}^{1/3} \rho_a^{-2/15} E_{\rm sn}^{-3/5} , \qquad (9)$$

assuming an ejecta exponent of $n = 9$. This ratio is $\sim$0.2 for our nominal parameters. Note that both of these pressures will be slightly lower: P_b because the pulsar has likely died out by the time of the collision, P_2 because the pressure in the driven wave will drop once the reverse shock starts falling to the center.

We have run additional models in order to show the effects of changing the energy in the pulsar bubble on the evolution of the PWN/SNR interaction. In model B we dropped the pressure ratio in equation (9) by a factor of $\sim$3 through a smaller ejecta mass (4 $M_\odot$) and smaller pulsar luminosity (10^{39} ergs s^{-1}). In model C the pressure ratio was increased by a factor of 2.4 by doubling the ejecta mass (16 $M_\odot$) and increasing the pulsar luminosity (5×10^{40} ergs s^{-1}). The evolution of all three models is shown in Figure 3. As expected, the lower the pressure in the pulsar bubble, the more the bubble is compressed by the reverse shock. In the lower pressure model the radius of the bubble after collapse is only $\sim$0.06 R_1 .

The evolution in the high-pressure model is slightly different since these parameters switch the ordering of t_2 and t_3. In this case the pulsar nebula hits the edge of the ejecta plateau at $\sim\tau$, well before the PWN/SNR collision. There is thus an intermediate phase when the pulsar shell accelerates down the steep ejecta gradient before impacting the SSDW. This results in a more violent collision, which compresses the SSDW by a factor of $\sim$2 and accelerates the forward shock considerably more than in the standard model. Despite this more violent beginning, however, the subsequent evolution is very similar to the standard model, albeit leaving behind a larger pulsar bubble.

It can be seen in Figure 3 that after the PWN has been crushed, the ratio R_p/R_1 evolves slowly with time, if the pressure wave induced oscillations are averaged out. If approximate pressure equilibrium is established between the PWN and the interior of the blast wave, we expect $R_p \propto t^{0.3}$ (RC84). The radius of a Sedov blast wave evolves as

$$R_1 = \left(\frac{2.025 E_{\rm sn}}{\rho_a}\right)^{0.2} t^{0.4} , \qquad (10)$$

so the slow evolution of R_p/R_1 is expected. Van der Swaluw & Wu (2001) have emphasized this point, noting that equating the pressure in the PWN with the interior pressure in the blast wave leads to

$$\frac{R_p}{R_1} = 1.02 \left(\frac{E_{\rm pwn}(t)}{E_{\rm sn}}\right)^{1/3} , \qquad (11)$$

where $E_{\rm pwn}(t)$ is the internal energy in the PWN at time t. We now assume that the pulsar power can be assumed to be constant up to time t_p, after which it falls to 0. The value of

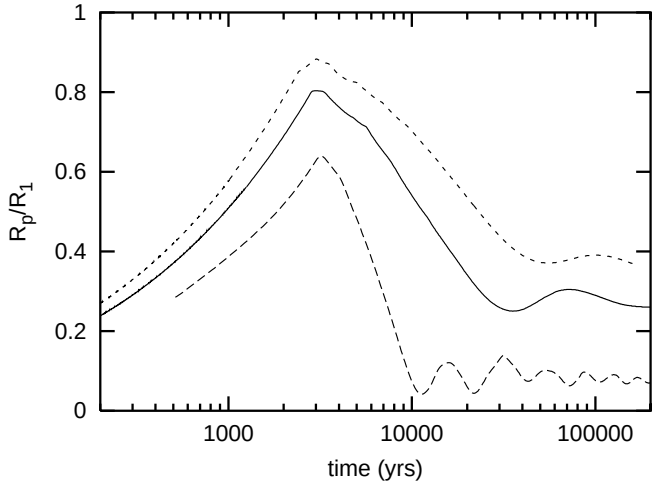

FIG. 3.—Evolution of the pulsar nebula through the return of the reverse SNR shock for the three different models listed in Table 1: model A (*solid*), model B (*long-dashed line*), and model C (*short-dashed line*). The radius of the pulsar nebula is scaled to the (increasing) radius of the SNR as in the previous figure.

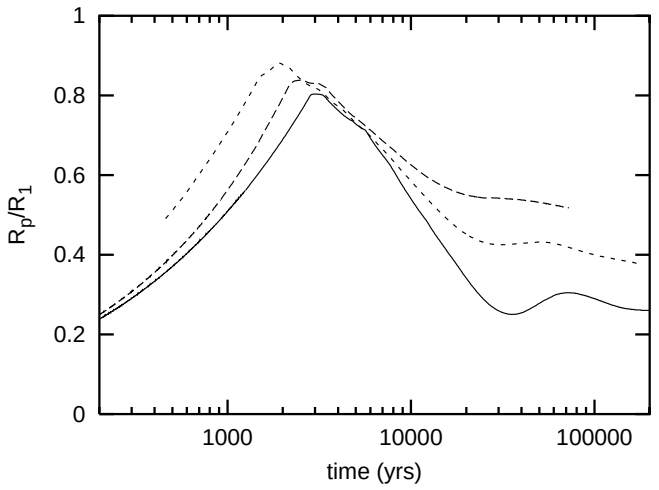

FIG. 4.—Evolution of the PWN for models A, D, and E listed in Table 1. The radius of the pulsar nebula is scaled to the (increasing) radius of the SNR as in the previous figure.

$E_{\rm pwn}(t)$ can be related to the total spin-down energy of the pulsar $E_{\rm sd} = L_{\rm pi} t_p$ for $p = 3$. During the initial expansion phase ($t \le t_p$), the radius of the PWN is given by equation (5) and $E_{\rm pwn}(t) = 5L_p t/11$ (RC84). For $t > t_p$, the evolution of the PWN is adiabatic, so that $E_{\rm pwn}(t) = E_{\rm pwn}(t_p)R_p(t_p)/R_p(t)$, where $E_{\rm pwn}(t_p) = 5E_{\rm sd}/11$. With the use of equations (5) and (10), equation (11) can be expressed as

$$\frac{R_p}{R_1} = 0.866\left(\frac{E_{\rm sd}}{E_{\rm sn}}\right)^{0.3} \times \left[\left(\frac{n-5}{n-3}\right)^{0.5}\left(\frac{n}{n-5}\right)^{0.2}\frac{E_{\rm sn}^{0.3}\rho_a^{0.2}t_p}{M_{\rm ej}^{0.5}}\right]^{0.25} t^{-0.1}. \quad (12)$$

Application of equation (12) to the three models discussed here yields $R_p/R_1 = 0.20$ (model A), 0.11 (model B), and 0.29 (model C) at $t = 1.6 \times 10^5$ yr if we take $t_p = \tau$. It can be seen from Figure 3 that these values are slightly lower than seen in the simulations. This discrepancy is due in large part to the time-dependence of L_p, such that some pulsar energy continues to be added to the bubble after a time τ. In simulations with a constant value of L_p up until t_p and zero thereafter, the radius of the crushed PWN at late times was better fitted by this approximation.

We have $E_{\rm sd} = I\Omega_i^2/2$, so that the observed value of R_p/R_1 can be related to the initial spin rate of the pulsar (van der Swaluw & Wu 2001); since $R_p/R_1 \propto \Omega_i^{0.6}$, the value of R_p/R_1 appears to be more sensitive to Ω_i than to the other uncertain parameters. However, there is some sensitivity to the power input timescale, $t_p \approx \tau$, because if τ is small, the wind power is injected at an early time and the bubble energy is more subject to adiabatic expansion losses. In the magnetic dipole model with braking index $p = 3$, τ in equation (6) is given by (e.g., Shapiro & Teukolsky 1983)

$$\tau = \frac{3Ic^3}{\Omega_i^2 B_{\rm ns}^2 R_{\rm ns}^6 \sin^2\alpha}, \quad (13)$$

where $B_{\rm ns}$ is the magnetic dipole field strength of the pulsar, $R_{\rm ns}$ is its radius, and α is the angle between the dipole field and the rotation axis of the pulsar. Ordinary radio pulsars appear to have magnetic field strengths in a fairly narrow range around 3×10^{12} G (e.g., Stollman 1987), comparable to the field strength of the Crab pulsar. There may be a separate class of strongly magnetized neutron stars, magnetars, with $B_{\rm ns} \gtrsim 10^{14}$ G (Duncan & Thompson 1992); these objects are expected to rapidly deposit their rotational energy into the surroundings. Turning to the initial spin rate and taking $t_p \approx \tau \propto \Omega_i^{-2}$ as given by equation (13), we have $R_p/R_1 \propto \Omega_i^{0.1}$. The insensitivity of R_p/R_1 to Ω_i is due to the fact that a pulsar with a large spin-down energy tends to deposit the energy into the nebula early, when it is subject to adiabatic expansion losses. In addition, early radiative losses can decrease the energy in the pulsar bubble (see also van der Swaluw & Wu 2001). The radiative luminosity of the Crab Nebula at present is $\sim\frac{1}{3}$ of the spin-down power (Davidson & Fesen 1985), and the higher magnetic field at earlier times can make the losses even more important. Atoyan (1999) has described a model for the Crab Nebula in which the initial period is $\sim$4 ms and most of the spin-down energy is lost to radiation. For these combined reasons, the observed value of R_p/R_1 for an evolved pulsar wind nebula is unlikely to lead to a reliable estimate for the initial spin rate.

To illustrate these effects we show, in Figure 4, the evolution of R_p/R_1 for three models with the same SNR parameters, but different pulsar winds. In particular, we include two models with the same total spin-down energy: model D, with $L_p = 5 \times 10^{40}$ ergs s^{-1} and $\tau = 500$ yr, and model E, with $L_p = 10^{40}$ ergs s^{-1} and $\tau = 2500$ yr. Equation (12) predicts that the pulsar with a more gradual power output will produce a PWN at late times that is 50% larger than a PWN from a pulsar with the same spin-down energy, but releasing it away 5 times faster.

In addition to the PWN, radiative cooling can be important for the outer SNR, resulting in the formation of a dense shell (Chevalier 1974; Cioffi, McKee, & Bertschinger 1988). The shell radius expands approximately as $R_1 \propto t^{0.3}$. If both the PWN and the hot interior SNR gas evolve adiabatically and $R_p^3 \ll R_1^3$, pressure equilibrium between the PWN and the SNR implies that $R_p^4 \propto R_s^5$ or $R_p/R_1 \propto t^{0.075}$. The size of the PWN nebula relative to the SNR again remains approximately constant with time, although now the PWN expands slightly more rapidly. The hot SNR gas may not evolve adiabatically but may be subject to radiative cooling just inside the dense shell (Chevalier 1974). This has the effect of further increasing the ratio R_p/R_1.

4. TWO-DIMENSIONAL HYDRODYNAMIC SIMULATIONS

4.1. *Evolution in a Uniform Medium*

To investigate the effects of instabilities on the morphology of the pulsar nebula, we have extended our models to two dimensions. We computed these models on a cylindrical (R-z) grid of 2000 × 2000 zones. We assume reflection symmetry about the equator and compute only one hemisphere. The initial conditions are taken from the first stage of the one-dimensional simulations just after the drop of the pulsar wind termination shock. In order to make these simulations more computationally efficient, we have raised the density in the pulsar bubble by a factor of 30. This artificially lowers the sound speed in the hot bubble allowing the use of a larger time step. Although this increases the time needed to equilibrate the pressure in the bubble, the sound crossing time is still relatively short compared to the expansion time, and one-dimensional simulations with and without this modification produced identical global evolutions. Again, we evolve this model on a moving grid

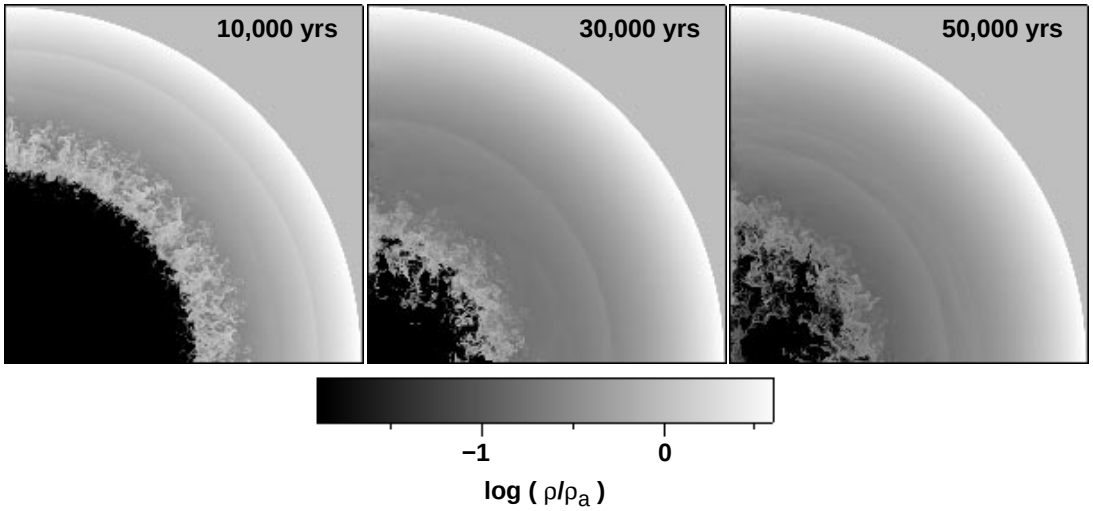

FIG. 5.—Crushing of the pulsar nebula in a two-dimensional simulation using the parameters for model A listed in Table 1. The length scale of the images is normalized to take out the expansion of the outer shock front. [*See the electronic edition of the Journal for a color version of this figure.*]

that follows the outer shock front, so that the full resolution of the grid is always used.

The outer shock front remains very nearly spherical and follows the time evolution of the one-dimensional model to within 0.1%. The key difference is the instability of the thin shell of ejecta and the rapid mixing driven by this instability. Even before the PWN/SNR interaction, the instability of the SSDW (Chevalier et al. 1992) begins to spread out the shell of shocked ejecta. However, given the short time between the beginning of the simulation and the crash of the reverse shock, there is not enough time for this instability to grow to significant amplitude. Following the PWN/SNR collision, the deceleration of the ejecta shell by the shocked ambient medium (responsible for the SSDW instability) increases in magnitude, thereby driving a more rapid Rayleigh-Taylor instability. The result is a broadened shell of mixed ejecta and ambient medium as seen in the first two frames of Figure 5.

Much more dramatic, however, is the Rayleigh-Taylor instability working in the opposite direction when the high pressure of the compressed pulsar bubble begins to accelerate the ejecta shell back outwards. From the one-dimensional simulation shown in Figure 2, we see that once R_p/R_1 drops below ~ 0.5, the pressure in the compressed PWN exceeds that in the SNR and the PWN begins to decelerate the shell of shocked ejecta. This acceleration of the dense ejecta gas by the low-density PWN gas is subject to the Rayleigh-Taylor instability. As a result of this instability, much of the ejecta gas continues toward the center of the SNR almost unabated. In the absence of a PWN, a spherical reverse shock would reach the center of the remnant at an age of ~ 35000 yr, and indeed we see in Figure 5 that some has reached the center by this time. In the same process some relativistic gas is displaced from the center.

We see two competing effects of this instability in the PWN crushing phase. First, as relativistic gas is displaced from the center, it escapes the full compression of the infalling ejecta seen in one dimension. Second, the vigorous turbulence driven by this instability leads to rapid mixing of the thermal and relativistic gasses. To illustrate these effects, we compare the effective value of R_p/R_1 in the one- and two-dimensional simulations in Figure 6. We compute the radius of the pulsar bubble in the two-dimensional simulation by summing up the volume of gas with $\gamma < 1.66$ (i.e., including the partially mixed gas) and calculate an effective radius assuming a spherical volume. Prior to the bounce, the one- and two-dimensional simulations are nearly identical. However, at the moment of bounce, the PWN in the two-dimensional simulation has a volume twice that of the PWN in the one-dimensional simulation. The compressed PWN quickly rebounds in the one-dimensional simulation, but in two-dimensions the volume of relativistic gas continues to shrink because of numerical mixing.

This rapid depletion of the volume of the PWN in the two-dimensional simulation is an artifact of numerical diffusion; when one numerical zone contains both relativistic gas ($\gamma = 4/3$) and ejecta gas ($\gamma = 5/3$), the mass-weighted average γ is dominated by the high density of the ejecta. As a result, the mixing—and subsequent loss of PWN volume—is strongly dependent on the numerical resolution of the simulation. Higher spatial resolution leads to less numerical mixing across the contact interface between the

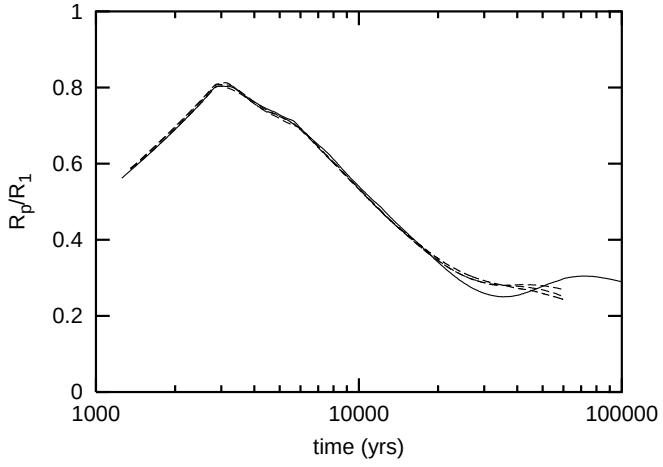

FIG. 6.—Evolution of the pulsar nebula through the crash of the reverse SNR shock in one (*solid line*) and two (*dashed lines*) dimensions with different numerical resolutions.

FIG. 7.—Rapid mixing of the thermal gas of the SN ejecta (*white*) and the relativistic gas of the PWN (*black*) is seen in these images of γ at a time of 50,000 yr, shortly after the bounce of the pulsar bubble in the corresponding one-dimensional simulation. The three images correspond to increasing numerical resolution, with the number of zones per dimension: $N = 500$ (*left*), 1000 (*center*), and 2000 (*right*).

two gasses, but it also leads to more vigorous hydrodynamic mixing by resolving the turbulence generated on smaller scales. The result of these competing effects can be seen in Figure 7, where we compare the distribution of relativistic gas in three two-dimensional simulations with varying resolutions. We also plot the effective value of R_p/R_1 for these three simulations in Figure 6. Up until a time of $\sim$35,000 yr, all three simulations are quite similar. Once the Rayleigh-Taylor instability kicks in, however, the resolution-dependent effects of mixing become quite evident. Independent of the numerical resolution, it is clear that the mixing of relativistic gas and thermal gas is very efficient.

4.2. *Evolution in Nonuniform Media*

We have repeated our two-dimensional simulation with the addition of a density gradient in the ambient medium with the goal of understanding the displacement of the pulsar bubble seen in the Vela SNR. Following Dohm-Palmer & Jones (1996), we use a smooth density distribution in the vertical direction given by

$$\rho(z) = \rho_c \left[1 - \frac{2 - x}{x} \tanh\,(z/H) \right], \qquad (14)$$

such that the density contrast, from a minimum at large positive z to a maximum at large negative z, is given by $(x - 1)^{-1}$, and H is the characteristic length scale over which the density changes. The simulations shown here use $x = 1.2$ corresponding to a density contrast of 5. These simulations require the computation of the full domain in z (i.e., no assumption of equatorial symmetry). As a result, our standard grid of 2000 zones represents only half the resolution used in the previous two-dimensional model.

In Figure 8 we show the evolution of the PWN/SNR system for an ambient medium length scale of $H = 1 \times 10^{19}$ cm, which corresponds to the size of the SNR at an age of $\sim$500 yr. Early in the evolution, we can estimate the asymmetry in the SNR by assuming only radial motion, such

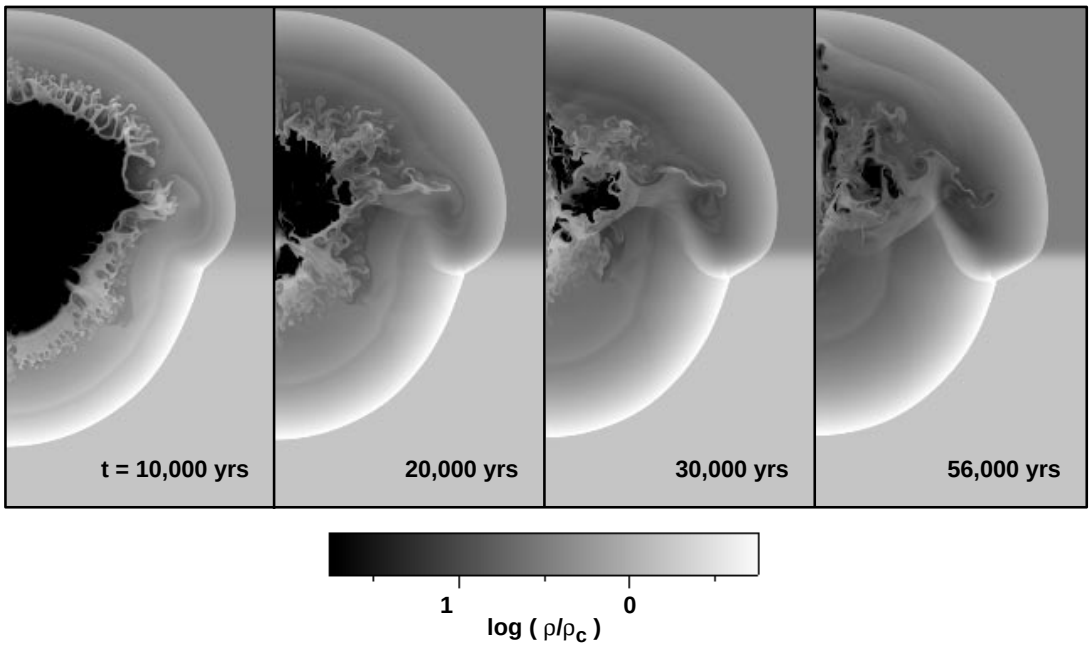

FIG. 8.—Evolution of the pulsar nebula/supernova remnant for the model with a scale height of $H = 1 \times 10^{19}$ cm in the ambient medium. [*See the electronic edition of the Journal for a color version of this figure.*]

that the local radius is determined by equation (4) with the local preshock density. The full density contrast of 5 thus produces a relatively minor ratio in radii at the poles of $5^{1/9} \approx 1.2$. The ratio of pressures behind the forward shocks is more pronounced: $5^{7/9} \approx 3.5$ Thus, while the forward shock is only mildly asymmetric, the interior pressure variation drives a substantial asymmetry in the process of crushing the PWN.

If the ambient medium had an exponential density distribution instead of a step in density, the distortion of the outer shock front would not be as apparent (e.g., Hnatyk & Petruk 1999). In Figure 9 we show the results of two additional simulations with larger values of H, but all at the same age of $\sim$50,000 yr. In the simulation with $H = 1 \times 10^{20}$ cm, the asymmetry in the CSM at the time of the PWN/SNR interaction is less than a factor of 2, and the crushed PWN is only slightly off-center. But a slightly steeper density gradient, $H = 3 \times 10^{19}$ cm, begins to affect the SNR prior to the PWN/SNR interaction, and the crushed PWN is displaced from the center of the remnant by roughly 40% the radius of the SNR.

5. COMPARISON WITH OBSERVATIONS

5.1. *The Vela Remnant*

A pulsar nebula that is likely to be in the post–reverse shock phase is Vela X in the Vela supernova remnant. This nebula was first identified as a region with a flat radio spectral index near the Vela pulsar (Weiler & Panagia 1980). More recent radio studies have shown that some of the emission is in filamentary structures as well as a diffuse background (Milne 1995; Frail et al. 1997; Bock, Turtle, & Green 1998). The extended Vela X emission is largely to the south of the pulsar and this, as well as uncertainties in the spectral index, has led to the suggestion that Vela X is part of the Vela shell (Milne & Manchester 1986; Gvaramadze 1998). However, the radio observations of Bock et al. (1998) give an especially detailed view of the Vela X nebula, and it appears to be distinctive compared to the rest of the shell. The overall appearance is chaotic, in keeping with the expected instabilities during the crushing and reexpansion phases in our model. There are a number of radio filaments, and the magnetic field lines lie along the filaments; this is expected if the Rayleigh-Taylor instability occurs primarily across the magnetic field rather than along it. In their Figure 5, Bock et al. (1998) show the projected velocity of the Vela pulsar, including the pulsar position 12,000 yr ago; it is near the north edge of the Vela X nebula. Even if this age is incorrect, the direction of the pulsar velocity cannot take it to the center of the nebula. We propose that the reason for the asymmetry is an asymmetry in the medium surrounding the supernova remnant.

The interstellar medium surrounding the Vela remnant is known to be inhomogeneous. From X-ray observations, Bocchino, Maggio, & Sciortino (1999) deduced the presence of various interstellar components, the lowest density component having a hydrogen density $n_{\rm H} \approx 0.06$ cm^{-3}. From H I observations, Dubner et al. (1998) deduced a preshock density $n_{\rm H} \approx 1$ cm^{-3}; this denser gas is primarily on the north side of the Vela remnant. We thus propose that the supernova occurred at the pulsar position (corrected for its velocity), that the higher density to north caused greater SNR expansion to the south, and that the asymmetry in the reverse shock front pushed the pulsar nebula to the south of the pulsar. The age of the remnant can be estimated from the spin-down age of the pulsar, $t_{\rm sd} = P/[(p-1)\dot{P}]$, where p is the pulsar braking index, P is the pulsar period, and $\dot{P}$ is its time derivative. The spin-down age is the actual age if p is constant, the pulsar magnetic field is constant, and the current spin rate is much less than the initial rate. If this last assumption is violated, the age is less than $t_{\rm sd}$. For the magnetic dipole model with $p = 3$, we have $t_{\rm sd} = 11{,}000$ yr for the Vela pulsar (Reichley, Downs, & Morris 1970). However, Lyne et al. (1996) found evidence for $p = 1.4 \pm 0.2$, which leads to a larger value of $t_{\rm sd} \approx 56{,}000$ yr. These estimates show consistency with the hypothesis that the reverse shock front has recently crushed the pulsar nebula in Vela. Another expectation of the reverse shock model is that the pressure in the pulsar nebula should be comparable to the pressure in the hot gas in the Vela remnant. Estimates of the pressure in the relativistic fluid from minimum energy synchrotron emission arguments show that this is approximately the case (Frail et al. 1997).

With the standard assumptions, the evolution of the pulsar spin rate is

$$\Omega = \Omega_i \left(1 + \frac{t}{\tau}\right)^{-1/(p-1)}, \qquad (15)$$

where Ω_i is the initial pulsar spin rate and τ is approximately the timescale for power input by the pulsar (see § 3).

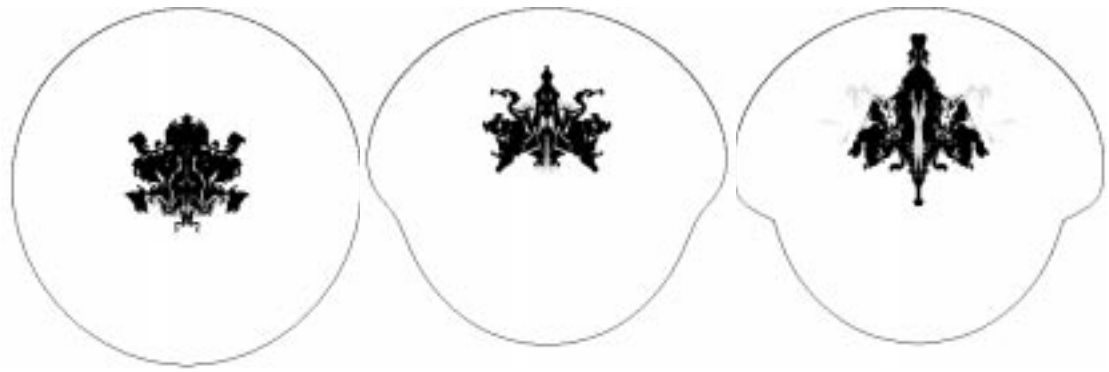

FIG. 9.—The remnants of the pulsar nebula as defined by the adiabatic index (black is gas with $\gamma < 5/3$) for simulations with a scale height of $H = 1 \times 10^{20}$ cm (*left*), $H = 3 \times 10^{19}$ cm (*center*), and $H = 10^{19}$ cm (right). The solid contours mark the location of the shock front. These snapshots are from a time of $\sim$50,000 yr, when the SNR has a radius of $\sim 1.5 \times 10^{20}$ cm.

The present period of the Vela pulsar is $P = 2\pi/\Omega = 89$ ms. If $p = 1.4$ and $t \gg \tau$, we have $\Omega \approx \Omega_i(t/\tau)^{-2.5}$ and the rapid evolution of the spin rate requires a value of the initial spin rate that is faster than plausible if $\tau \approx 500$ yr. This is true even for our model E, with $\tau \approx 2500$ yr. However, the value of $p = 1.4$ by Lyne et al. (1996) is uncertain because of the frequent glitching of the pulsar and a value closer to the magnetic dipole value of 3 is possible. Of the models presented in § 3, model A appears most suitable because the radius of the pulsar nebula is $\frac{1}{4}$ of the outer shock radius after the crushing has occurred; the diameter of Vela X is $\sim 2^\circ$ (Bock et al. 1998), as compared to the $\sim 8^\circ$ diameter of the Vela SNR.

The fact that the Vela pulsar is to one side of Vela X has led to previous discussions of how power might flow from the pulsar into the Vela X region. Observations with *ROSAT* have shown an X-ray filament to the south of the pulsar that has been interpreted as emission from a jet extending from the pulsar (Markwardt & Ögelman 1995). It is not yet clear whether the X-ray emission is thermal or nonthermal (Markwardt & Ögelman 1997). Frail et al. (1997) suggested that some of the radio structures are related to the X-ray "jet." However, the radio filament near the X-ray feature appears to be similar to other radio filaments in the Vela X region (Bock et al. 1998). Also, the X-ray spectrum of the feature is similar to that of the more diffuse X-ray emission in the Vela X region (Markwardt & Ögelman 1997). Wijers & Sigurdsson (1997) noted difficulties with the high momentum in the proposed X-ray jet and suggested a different model combining fallback onto the neutron star with a trail left by a high-velocity binary companion.

The model described here suggests a different interpretation of the "jet" features. As mentioned above, the linear feature in the radio synchrotron emission can be the result of the Rayleigh-Taylor instability during the crushing process. The instability also results in hot, thermal gas being mixed into the region initially occupied by the relativistic fluid. Because of the sweeping action of the pulsar nebula, the gas immediately outside the pulsar nebula has a higher density than that occupying most of the SNR (Figs. 1 and 2). It is thus plausible that some of the gas mixed into the pulsar nebula has a higher emissivity and appears as an X-ray filament. Frail et al. (1997) found that the radio and X-ray emission are not coincident but lie near each other, as would be expected in our model.

5.2. *Other Remnants*

The return of a reverse shock front to the center of a supernova remnant is not generally expected to be spherically symmetric because of inhomogeneities in the surrounding medium. Thus we might expect our models to be broadly applicable to composite supernova remnants which have both an apparent pulsar nebula and a well-developed shell (see Helfand 1998 for a list of objects). The radio-emitting electrons are long-lived and are the best tracer of the power input from the pulsar during its phase of high power output. The X-ray–emitting electrons are shorter lived and provide an indication of the current position of the pulsar, even if a pulsar has not been directly observed. However, an observable shell may be present before the reverse shock crushing phase. This appears to be the case, for example, in the Large Magellanic Cloud remnant 0540–69, which has a pulsar nebula very similar to the Crab Nebula (Kaaret et al. 2001). At late times, the mixing of the radio-emitting electrons with the thermal gas may lead to the disappearance of the radio nebula from the initial injection phase. In this case, only emission from near the pulsar, likely to be in a trail because of the pulsar velocity, is present.

In the Vela remnant, the pulsar is surrounded by an X-ray PWN, while the radio-emitting PWN is displaced from the X-ray emission. A similar situation appears to be present in the remnants MSH 15−56 (G326.3−1.8; Plucinsky 1998; Gaensler 2001), G327.1−1.1 (Sun, Wang, & Chen 1999), and G0.9+0.1 (Gaensler, Pivovaroff, & Garmire 2001) although pulsars associated with the X-ray emission have not yet been discovered in these cases. Another case with a pulsar (PSR B1643−43) is G341.2+0.9 (Giacani et al. 2001). The broad regions of radio emission are excellent candidates for wind nebulae injected early in the pulsar evolution and crushed by the reverse shock.

A less clear-cut case is the PWN inside W44 (Frail et al. 1996; Harrus et al. 1996). The radio nebula has a bow shock appearance, but the trailing emission is considerably broader and stronger than that near the pulsar. The ratio of PWN radius to outer shock radius is ~ 0.1. Although smaller than the case of Vela, this situation is expected in our models (see Fig. 3). The age of W44 is $\sim$20,000–30,000 yr, but the relatively high density of its surroundings places it in a more evolved category than Vela (Chevalier 1999). Another remnant with relatively dense surroundings is IC 443, with an estimated age of 30,000 yr (Chevalier 1999). Early radio spectral observations indicated the presence of a PWN (Green 1986), and recent X-ray and radio observations clearly show a bow shock nebula with a compact X-ray source at the head (Olbert et al. 2001). In this case, the radio emission region is narrow and is strongest close to the compact X-ray source; there is no clear sign of emission from a remnant nebula that has been crushed by the reverse shock front. The trailing emission is an approximately linear feature, but does not point toward the center of the remnant. This appears to be another case of an off-center explosion due to asymmetries in the surrounding medium. This situation may account for some of the high velocities deduced for pulsars from their positions relative to what appears to be their parent SNR (Frail, Goss, & Whiteoak 1994).

6. DISCUSSION AND CONCLUSIONS

We have considered the evolution of PWNs inside supernova remnants, with special attention to the effect of the reverse shock front on the PWN. It is possible that synchrotron losses are important for the PWN at early times, but they are unlikely to be significant at the times of interest here, and the effect can be approximately accounted for by renormalizing the pulsar spin-down energy. We do not treat the instabilities that can occur early in the evolution as a result of the acceleration of the shell outside the pulsar nebula (Jun 1998); these would only further contribute to the instabilities that we find later in the evolution.

Our simulations allow for two fluids: a $\gamma = 4/3$ fluid for the PWN and a $\gamma = 5/3$ fluid for the surrounding gas. We do not allow for the magnetic field that is expected to be mixed in with the relativistic particles and that can influence the evolution through magnetic tension. The field might affect the Rayleigh-Taylor instabilities that occur when the PWN is compressed by the reverse shock gas and subse-

quently reexpands. The magnetic field can dampen the instability along magnetic field lines, but not across them, leading to the creation of filaments along the magnetic field direction. There is mixing between the fluids so that the separation of the two fluids depends on the numerical resolution of the two-dimensional simulations. The degree of mixing may also depend on the magnetic field.

In addition to causing mixing of thermal gas with the PWN, the reverse shock wave is unlikely to be spherically symmetric and can thus push the PWN off-center from the explosion site. The position of a pulsar can be displaced from the explosion site both because of this effect and because of the velocity that the pulsar acquires at birth.

In comparing the model results with observations, it is important to correctly identify the evolutionary state of a PWN. During the initial phase when the PWN is interacting with the freely expanding supernova ejecta, the pulsar is expected to be approximately centrally located within the PWN. Even if the pulsar has a significant velocity, it will not have a particular position in the uniformly expanding medium unless there is a large density gradient in the medium. Nebulae likely to be in this phase include the Crab Nebula and 3C 58.

The next event in the evolution is the cessation of power input from the central pulsar. The outer edge of the nebula continues its free expansion, leading to a low surface brightness nebula that can have a substantial filling fraction within the external shock wave. The nebula MSH 15−52 around the pulsar PSR B1509−58 (Seward et al. 1984) may be in this phase.

Here we have emphasized the late evolutionary phase after the reverse shock front comes back to the center of the remnant. An excellent candidate for this phase of evolution is the Vela X radio remnant within the Vela supernova remnant. The fact that the pulsar nebula is displaced from the pulsar can be explained in our model without the need for directed power from the pulsar. Asymmetries in the placement of radio PWNs relative to their pulsars are likely to be common in this phase because the interstellar medium is generally inhomogeneous.

Support for this work was provided in part by NASA grants NAG 5-8130 and NAG-7153. The hydrodynamic simulations were computed on an IBM SP at the North Carolina Supercomputing Center.

REFERENCES

Atoyan, A. M. 1999, A&A, 346, L49
Bocchino, F., Maggio, A., & Sciortino, S. 1999, A&A, 342, 839
Bock, D. C.-J., Turtle, A. J., & Green, A. J. 1998, AJ, 116, 1886
Chevalier, R. A. 1974, ApJ, 188, 501
———. 1977, in Supernovae, ed. D. N. Schramm (Dordrecht: Reidel), 53
———. 1982, ApJ, 258, 790
———. 1998, Mem. Soc. Astron. Italiana, 69, 977
———. 1999, ApJ, 511, 798
Chevalier, R. A., Blondin, J., & Emmering, R. T. 1992, ApJ, 392, 118
Cioffi, D. F., McKee, C. F., & Bertschinger, E. 1988, ApJ, 334, 252
Davidson, K., & Fesen, R. A. 1985, ARA&A, 23, 119
Dohm-Palmer, R. C., & Jones, T. W. 1996, ApJ, 471, 279
Dubner, G. M., Green, A. J., Goss, W. M., Bock, D. C.-J., & Giacani, E. 1998, AJ, 116, 813
Duncan, R. C., & Thompson, C. 1992, ApJ, 392, L9
Emmering, R. T., & Chevalier, R. A. 1987, ApJ, 321, 334
Frail, D. A., Bietenholz, M. F., Markwardt, C. B., & Ögelman, H. B. 1997, ApJ, 475, 224
Frail, D. A., Giacani, E. B., Goss, W. M., & Dubner, G. 1996, ApJ, 464, L165
Frail, D. A., Goss, W. M., & Whiteoak, J. B. Z. 1994, ApJ, 437, 781
Gaensler, B. M. 2001, in Young Supernova Remnants, ed. S. S. Holt & U. Hwang (New York: AIP), 295
Gaensler, B. M., Pivovaroff, M. J., & Garmire, G. P. 2001, ApJ, 556, L107
Giacani, E. B., Frail, D. A., Goss, W. M., & Vieytes, M. 2001, AJ, 121, 3133
Green, D. A. 1986, MNRAS, 221, 473
Gvaramadze, V. V. 1998, Astron. Lett., 24, 144
Harrus, I. M., Hughes, J. P., & Helfand, D. J. 1996, ApJ, 464, L161
Helfand, D. J. 1998, Mem. Soc. Astron. Italiana, 69, 791
Hester, J. J., et al. 1996, ApJ, 456, 225
Hnatyk, B., & Petruk, O. 1999, A&A, 344, 295
Jun, B.-I. 1998, ApJ, 499, 282
Jun, B.-I., Norman, M. L., & Stone, J. M. 1995, ApJ, 453, 332
Kaaret, P., et al. 2001, ApJ, 546, 1159
Kennel, C. F., & Coroniti, F. V. 1984a, ApJ, 283, 694
———. 1984b, ApJ, 283, 710
Lyne, A. G., & Lorimer, D. R. 1994, Nature, 369, 127
Lyne, A. G., Pritchard, R. S., Graham-Smith, F., & Camilo, F. 1996, Nature, 381, 497
Markwardt, C. B., & Ögelman, H. 1995, Nature, 375, 40
———. 1997, ApJ, 480, L13
Milne, D. K. 1995, MNRAS, 277, 1435
Milne, D. K., & Manchester, R. N. 1986, A&A, 167, 117
Olbert, C. M., Clearfield, C. R., Williams, N. E., Keohane, J. W., & Frail, D. A. 2001, ApJ, 554, L205
Plucinsky, P. P. 1998, Mem. Soc. Astron. Italiana, 69, 939
Reichley, P. E., Downs, G. S., & Morris, G. A. 1970, ApJ, 159, 35
Reynolds, S. P., & Chevalier, R. A. 1984, ApJ, 278, 630
Seward, F. D., Harnden, F. R., Jr., Symkowiak, A., & Swank, J. 1984, ApJ, 281, 650
Shapiro, S. L., & Teukolsky, S. A. 1983, Black Holes, White Dwarfs, and Neutron Stars (New York: Wiley)
Stollman, G. M. 1987, A&A, 178, 143
Sun, M., Wang, Z.-R., & Chen, Y. 1999, ApJ, 511, 274
van der Swaluw, E., Achterberg, A., Gallant, Y. A., & Tóth, G. 2001, A&A, in press (astro-ph/0012440)
van der Swaluw, E., & Wu, Y. 2001, ApJ, 555, L49
Weiler, K. W., & Panagia, N. 1980, A&A, 90, 269
Wijers, R. A. M. J., & Sigurdsson, S. 1997, MNRAS, 290, 276